# Numerical Calculation of Self-Focusing and Trapping of a Short Light Pulse in Kerr Liquids

Abstract: Self-focusing and trapping of an intense, short light pulse is discussed on the basis of a parabolic scalar wave equation which includes a quadratic nonlinear refractive index. When the finite relaxation time of the nonlinear index is taken into account, the propagation properties of the transient solution differ considerably from those of the time-independent solution. Based mainly on the results of our numerical calculations, we show that contraction of the self-focusing pulse stops at a finite radius and that part of the pulse remains trapped beyond this focal point. The limiting radius decreases rather rapidly with increasing input power as well as with pulse width. However, if we assume a cutoff radius, the resulting filament accounts for experiments performed with multimode lasers. Effects of stimulated Raman scattering and dispersion are also discussed.

#### Introduction

The purpose of this paper is to show that various phenomena associated with the self-focusing of intense light pulses in Kerr liquids that are excited by multimode or mode-locked lasers can be explained rather naturally on the basis of the simplest wave equation having a quadratic nonlinear term. If phenomena in the very short time region of several picoseconds are ignored, bright spots and streaks observed in self-focusing are known [1,2] to be the tracks of the focal points which move through the medium in accordance with the change in light intensity. On the other hand, many observations, especially those obtained with multimode lasers, show evidence of optical "filament" formation. It has been understood that this trapping is a transient phenomenon, possibly associated with the finite response time of the optical Kerr effect. A model for the transient filament has also been proposed [3]. But the kind of formulation sufficient to explain transient phenomena remained unknown. Consequently, we have numerically integrated the equations proposed by Fleck and Kelley [4], which describe the propagation of a cylindrically symmetric light pulse in a nonlinear medium with finite relaxation:

$$\left(\frac{\partial}{\partial z} + \frac{1}{v_o} \frac{\partial}{\partial t}\right) E = i \left(\frac{\partial^2}{\partial r^2} + \frac{1}{r} \frac{\partial}{\partial r}\right) E + i \chi_{\rm NL} E, \tag{1}$$

$$\frac{\partial \chi_{\rm NL}}{\partial t} + \chi_{\rm NL} = |E|^2,\tag{2}$$

The calculations enable us to explain certain commonly observed phenomena in self-focusing in liquids which were not found by the authors of Ref. 4 because of limitations in their numerical calculations. In the above equations the time t is normalized by the relaxation time of the nonlinear refractive index  $\chi_{\rm NL}$ , and z by  $2ka^2$ , where k is the linear wave vector in the medium. The radial normalization factor a may be chosen arbitrarily. In the following numerical integrations it is usually the 1/e power radius of the input Gaussian beams. The field amplitude E is normalized by  $(\epsilon_0/\epsilon_2)^{\frac{1}{2}}/ka$ , where the steady state nonlinear index is expressed as  $\epsilon_0^{\frac{1}{2}}|E|^2/2k^2a^2$ .

In the next section some previously published experimental results are briefly reviewed. In the third section the time-independent theory is discussed and the reasons clarified for considering the transient character of the problem. Numerical results for Eqs. (1) and (2) are given in the fourth section, showing how these formulations provide an appropriate model for observed trapping phenomena. Dispersion effects and stimulated Raman scattering are then discussed in the final section.

The beam breakup problem [5-10], which is outside the scope of the cylindrical equation, (1), is not treated. We do not prove or disprove the existence of particular types of optical "filaments" that have been proposed in the past. But we do try to explain the most commonly observed phenomena in well-investigated liquids, such

as  $CS_2$  or benzene, on the basis of a simple model with a quadratic nonlinear refractive index.

### **Experimental observations**

The most immediate evidence of self-focusing of multimode lasers is obtained from observations of the spatial structure of the laser beam that emerges from a nonlinear liquid. The beam contains a large number of small bright spots which could not be seen at the entrance of the liquid cell [11,12]. These bright spots are usually formed from several millimeters to several centimeters away from the entrance of the light into the nonlinear liquid. The spots usually disappear if the path length in the cell is longer than 50 to 100 cm. The total energy of a spot ranges between 1 and 10 ergs, and the diameter varies from 5 to 10 \mum. These values depend on the medium as well as on the characteristics of the laser. For some spots the persistence time can be estimated from the modulation observed in the frequency spectrum [13,14]. The result is usually several picoseconds. Shorter durations of about 1 ps have been observed with a Nd mode-locked laser [15].

The question has been asked whether the bright spots result from rod-shaped trapped regions of the beam propagating through the liquid [1,2,16]. For a mode-locked laser it was clearly shown, from the time-resolved side picture of induced birefringence [15], that the trapped region actually propagates as much as several centimeters. For other types of lasers there was no definite experimental verification. The radial uniformity of the modulation pattern in the frequency spectrum [13,14,17], however, strongly suggested that the bright spots produced in this case also had a similar origin. The trapped region seemed to have a more or less uniform radius, though the existing experimental results were not accurate enough to discuss the detailed shape of the region.

The field intensity in those filaments can be estimated from the above data. Using typical values, 5  $\mu$ m for the radius, 5 ps for the duration, and 1 erg for the energy (values appropriate to CS<sub>2</sub>), the intensity is calculated to be 10<sup>11</sup> W/cm<sup>2</sup>. The refractive index change is then approximately  $3 \times 10^{-3}$  [18]. This value is also supported by other observations. The emission angle of the anti-Stokes rings in stimulated Raman scattering is slightly smaller than the longitudinal wave-matching direction. The difference corresponds to the same refractive index change [19,20]. The frequency broadening of filaments in CS<sub>2</sub> extends up to 10 or 20 percent of the laser frequency. If we assume an index increase of 10<sup>-3</sup>, the required propagation distance to produce such broadening is 5 to 10 cm, which is close to the maximum propagation distance of filaments observed experimentally with a mode-locked Nd laser [15].

These experimental values strongly suggest that Eqs. (1) and (2) should describe filament formation fairly well. For an index change of  $10^{-3}$  the lowest-order nonlinear index should be sufficient. The radius observed should also be large enough to justify treating the optical field as a scalar field. Finally, the second derivative of z can be ignored, since the focusing distance is relatively long.

It should be emphasized that not all the observed spots are filaments. Even for mode-locked lasers, bright spots are also observed by focusing the camera inside the cell [15]. This means that some spots are strongly scattering regions. In the fourth section it is explained that scattering regions should exist if Eqs. (1) and (2) are to describe filaments having the observed diameter. Furthermore, the streaks of light observed from the side cannot be considered as parts of filaments. The small total energy of a filament could not produce a very strong scattering. It is important, for the proper understanding of the phenomenon, to note that the energy in the trapped region is only a fraction of the total laser energy that participates in the self-focusing process.

# Time-independent solutions

A review is given in this section of time-independent results obtained with Eq. (1) and the instantaneous quadratic response

$$\chi_{\rm NL} = |E|^2. \tag{3}$$

Chiao, Garmire and Townes [21] have shown numerically that there exists a steady state solution in which the optical field propagates in the medium without change in its cross-sectional shape. The scaling characteristics of the equations indicate that the solution could take any radial size, provided the beam power is kept constant:

$$P = 2\pi \int_0^\infty r|E|^2 dr = P_{\rm th} = 5.85$$

The threshold power  $P_{\rm th}$  may be considered as the power level at which the focusing effect due to the nonlinear refractive index  $\chi_{NL}$  exactly cancels the radial expansion of the beam that is due to linear diffraction. When P is larger than  $P_{th}$ , and if the incoming beam is collimated and has a smooth radial shape, the beam collapses at a finite distance  $z_f$ . For high power the self-focusing distance  $z_f$  varies proportional to  $P^{-\frac{1}{2}}[22]$ . When P is slightly smaller than  $P_{th}$ , the beam can remain at an approximately constant radius many times its diffraction length before diverging again [23]. This is particularly true for prefocused beams. The radial size of the beam in this elongated focal region is then much smaller than the radius at the linear focal point. However, the input power range in which the focal region can be regarded as a trapped filament is very small [23].

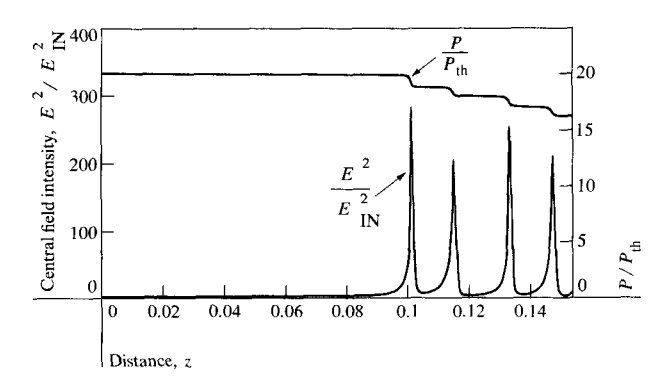


Figure 1 Multiple focusing with a cubic loss (see text). The two curves show the development of the intensity at the center and of the total beam power P. Each time the beam self-focuses, it loses energy approximately equal to the threshold power  $P_{\text{th.}} |E|_{\text{III}}^2$  is the square of the input field in the center.

As far as the self-focusing distance is concerned, the agreement with experiments is relatively good. In early experiments the approximate relation  $z_f \propto P^{-\nu_2}$  was verified [24]. However, the self-focusing solution of Eqs. (1) and (3) does not lead to the kind of trapped filament that was thought to be the source of the bright spots observed. The solution has been shown to collapse rather than to stabilize to a finite radius [22]. In fact, the steady state solution has been reported to be unstable against small perturbations [10].

In view of the large field intensity, saturation of the nonlinear index was first considered as a mechanism to limit the radius and to lead to a stable filament [25,26]. If Eq. (3) is replaced by a real function of  $|E|^2$ ,

$$\chi_{\rm NL} = f(|E|^2),\tag{4}$$

which is linear at small  $|E|^2$  and saturates at large  $|E|^2$ , one can usually obtain steady state solutions for all power levels above  $P_{th}[26]$ . In this case the radial size has a unique relation to P. When the index change is due to the reorientational Kerr effect, the radius becomes almost constant at higher power. The calculated size, however, is more than one order of magnitude smaller than the observed spot radius [26]. A more serious difficulty is that the solution of Eqs. (1) and (4) does not usually lead to a trapped state beyond the focal point. The beam has been observed to diverge and focus alternately [27,28]. This behavior is qualitatively understandable from the symmetry of Eq. (1). If the phase of the electric field is constant in the focal plane, the solution is symmetric across this plane. This condition is approximately satisfied for a relatively low input power. If the input power is made extremely high compared to  $P_{\rm th}$ , the phase at  $z_{\rm f}$  becomes rather complicated and, in this case, so is the behavior of the beam [28].

Nonlinear absorption could be considered as an alternative mechanism to stop beam collapse. The results of

numerical integration have an amazing resemblance to the solutions for the case of index saturation. The beam ceases to collapse and multiple foci are produced. Fig. 1 shows numerical results for a third-order nonlinear loss,

$$\chi_{\rm NL} = |E|^2 - i\alpha_1 |E|^4. \tag{5}$$

The input beam has a Gaussian shape and 20 times the threshold power. The loss coefficient  $\alpha_1 = 0.01$  was chosen arbitrarily to limit the radius contraction at around 10<sup>-2</sup>. The curves show the development of the central intensity and of the total beam power and are normalized to the input value and to  $P_{th}$ , respectively. Repeated focusing is clearly seen [29] in the figure. At each focal region the beam loses power by an amount approximately equal to  $P_{th}$ . A diffracted wave with large angle starts simultaneously from the same region, interfering with the field in the wing, which is still focusing. As the beam repeatedly focuses and defocuses, the field in the wing develops a rather complicated interference pattern. Numerical integration has not been continued beyond the fifth focal region because the existence of the largeangle scattered wave made further integration too timeconsuming. At higher input power, or higher loss, the solution does not show clean, repeated focusing, as is seen in Fig. 1. Under these conditions, an appreciable variation of the phase occurs around the center of the beam at the focal point. This is similar to the case of refractive index saturation [28]. The results with  $|E|^6$  and  $|E|^{s}$  losses are qualitatively similar to those with a thirdorder loss. Repeated focusing was not found with a second-order loss term  $|E|^2$ .

Only a part of the total power focuses at each focal region. In the geometrical-optics approximation this was explained as the aberration of self-focusing [27,30]. The numerical solution of Eqs. (1) and (3) seems to indicate that problems of stability are also involved. The beam shape near its center has a strong tendency to approach the steady state trapped solution as z approaches  $z_{\rm f}$  regardless of its input shape or power [29]. This tendency is clearly seen if one looks at the power contained inside the 1/e power radius near the focal point. Fig. 2 shows the variation of the self-focused power  $P_{tp}$  of a Gaussian-shaped input beam as a function of the central field intensity, where  $P_{\rm tp}$  is defined as  $\pi$  times the 1/epower radius times the square of the central field amplitude. Five curves are drawn for five input powers  $10^{n/2}P_{\rm th}$ , where n runs from 1 to 5. At the entrance to the medium  $P_{tp}$  is equal to the input power, corresponding to the left end of each curve. As the beam propagates and increases in intensity at the center,  $P_{tp}$  decreases rapidly. Even when the input power is larger than  $100P_{th}$ ,  $P_{tp}$  approaches the value 0.78  $P_{th}$ , which is the value of  $P_{\rm tp}$  corresponding to the steady state solution.

Examination of the beam shape near  $z_f$  also shows that it approaches the steady state shape rather than a Gaussian one. The same evolution was observed for other input shapes: Lorentzian, quadratic and exp  $(-r^4)$ .

These results should be kept in mind when considering the gain in any stimulated scattering process which is accompanied by the self-focusing. The over-all stimulated gain can increase to infinity only very slowly, as the radius at the focal point approaches zero. When the beam contraction stops at a finite value, the gain enhancement due to self-focusing is not always larger than that which could be produced by linear focusing. In a linear medium the over-all gain of stimulated scattering for a focused Gaussian beam is proportional to

$$\exp \left\{ g_s \int_{-\infty}^{\infty} |E| dz \right\} = \exp \left( 2Pg_s \right), \tag{6}$$

where  $g_s$  is an approximately normalized gain coefficient for the stimulated scattering.

This result is independent of the radial size at focus, or of the focal length of the lens. Although the formula is invalid for nonlinear focusing, the gain calculated from numerical solutions is not far from the over-all gain, Eq. (6), where P is now replaced by  $P_{\rm th}$ . For example, in the solution of Fig. 1 the gain in a single focal region is approximately exp 4  $P_{\rm th}g_{\rm s}$ , whereas the linear focusing is exp 40  $P_{\rm th}g_{\rm s}$ . Therefore, in a truly steady state situation the self-focusing of a beam will enhance the stimulated scattering gain only if the cell length is much shorter than a distance approximately equal to the linear diffraction length of the incoming beam.

### **Transient solutions**

The discussions in the previous sections indicate that time-independent theories are inadequate to account for experimental evidence of beam trapping. It should be noted that definite experimental evidence of trapping has usually been obtained for very fast phenomena in the time range of  $10^{-11}$  s. Since the relaxation time of the reorientational Kerr effect is of that order of magnitude, transient effects cannot be neglected [30-36]. In this section Eqs. (1) and (2), which provide the simplest description including a relaxation time, are shown to constitute an appropriate model to explain observed trapping phenomena.

One has to be careful when applying terms that usually specify propagation characteristics of a stationary light beam to a light beam changing rapidly in time. In this paper we use terms like "focusing" and "trapping" as terms that specify spatial propagation characteristics of each temporal part of a light pulse. A part of a light pulse may be called "trapped" if that part of the pulse propagates in the medium without changing its radius much beyond the linear diffraction length. Equations (1)

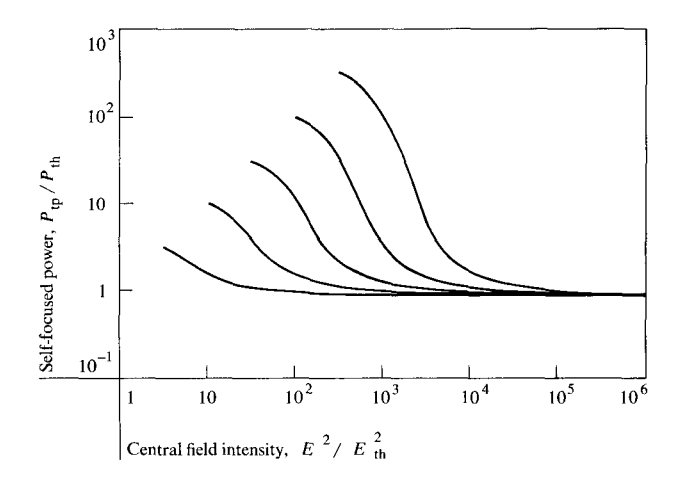


Figure 2 Change of the self-focused power  $P_{\rm tp}$  with the intensity at the center. Five curves are for input powers  $10^{n/2}P_{\rm th}$ , where  $n=1,2,\cdots,5$ . The self-focused power  $P_{\rm tp}$  is equal to the input power of the Gaussian beam at the entrance to the medium, corresponding to the left end of each curve. As the beam focuses, for all input powers  $P_{\rm tp}$  approaches 0.78  $P_{\rm th}$ , which is equal to the value for the steady state trapped case. The central field intensity is normalized to the field  $E_{\rm th}$  of a Gaussian beam having power  $P_{\rm th}$  and the input radius.

and (2) guarantee that each temporal part of a pulse can be distinguished from other parts throughout the propagation in the nonlinear medium, because each part of the pulse propagates with identical velocity  $v_{\rm g}$ . There is no ambiguity, therefore, in the above definition. It should be noted that, contrary to the stationary case, trapping of a light pulse does not necessarily mean the existence of a rod-shaped light beam having uniform radius. Various parts of the pulse can be trapped at different radii. The term "filament" is used in a less restrictive way. It specifies the part of a pulse which has roughly a rod shape and is trapped in the above sense. It will be shown that the filaments obtained by numerical integrations in this section have complex structures.

#### • Changes in pulse radii

The effect of the finite relaxation time is that  $\chi_{\rm NL}(t)$  is not determined by the instantaneous intensity  $|E(t)|^2$ , but rather by past values integrated over a time period of the order of the relaxation time. In consequence,  $\chi_{\rm NL}$  is zero at the leading edge of the pulse. Another important consequence is that  $\chi_{\rm NL}$  at a given space-time point is affected by previous temporal variations of the pulse shape at the same radial point.

The propagation of a pulse that is square-shaped in time and has a power larger than  $P_{\rm th}$  is described as follows. The front edge diverges according to normal, linear diffraction. The following portion starts to contract and contracts faster towards the tail. Linear diffraction increases as the radius decreases. In the case of instan-

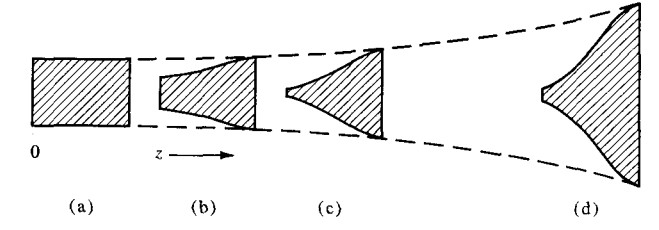


Figure 3 A schematic diagram of pulse propagation. (a) Input pulse; (b) the tail starts to contract; (c) the pulse reaches its limiting radius; (d) from (c) on, the pulse expands proportional to the linear diffraction of its leading edge. The dashed line indicates linear diffraction.

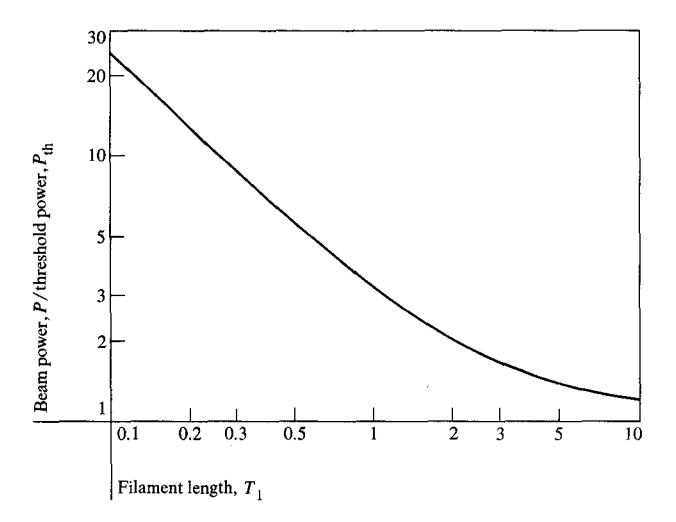


Figure 4 The filament length  $T_1$  as a function of beam power, from the steady state solution with finite relaxation time.

taneous response this is exactly compensated for by an increase of the focusing effect, since  $\chi_{NL}$  is inversely proportional to the square of the radius. With a finite relaxation time, however, the situation is somewhat different. The decrease in radius simultaneously enhances the temporal variation at a given radial point. Since  $\chi_{NL}$ is determined by the integral intensity, the increase in  $\chi_{\rm NL}$  is then insufficient to compensate for the increase in diffraction. As a result, the diffraction and the focusing effects balance when the variation in radius becomes sufficiently fast. From this point on, the entire pulse gradually expands approximately at the same rate as the expansion of the front edge. If the radius of the tail end is much smaller than the radius of the front end, the tail propagates many times its linear diffraction length without an appreciable change in radius. One may say that this part of the pulse is trapped. The schematic picture of such a propagation is represented in Fig. 3.

The existence of a finite rate of change of radius for which linear diffraction will balance against the focusing effect is justified by the existence of a steady state solution. It is easy to verify by substitution that E and  $\chi_{\rm NL}$  have solutions to Eqs. (1) and (2) of the forms

$$E = \kappa f(\kappa r) \exp(i\Lambda \kappa^2 z) \text{ and}$$
 (7)

$$\chi_{\rm NL} = \kappa^2 g(\kappa r), \tag{8}$$

with 
$$\kappa = \exp \left[ (t - z/v_g)/T_1 \right]$$
,

where  $\Lambda$  and  $T_1$  are constants, and f and g are real functions. This solution has a constant power at all times and propagates without change in its intensity profile. Numerical integration shows that a solution of Eqs. (1) and (2) of the form (7), with a finite cross-sectional power, exists for powers above threshold  $P_{th}$ . The constant  $T_1$  is a measure of the time during which the beam retains an approximately constant radius. The constant can be considered as the filament duration at the pulse tail. The power dependence of  $T_1$  is shown in Fig. 4. At high power, T, decreases almost linearly with  $P^{-1}$ . The existence of a solution of the form of Eq. (7) implies that a focusing pulse will stop contracting, at least in the mathematical sense, at some finite intensity. Furthermore, it is easy to see why previous attempts [4] to stabilize the filament radius by this mechanism have failed. Because the limiting pulse shape is an exponential horn, one must take a sufficiently fine grid size in the numerical integration to prevent an apparent divergence for input pulses of arbitrary length and intensity.

## • Stabilization of pulse radius

The question remains as to whether the focusing pulse does stabilize to a finite radius. It was shown in the last sections that, with instantaneous saturation, the beam diverges back beyond the focal point. With finite relaxation time the steady state solution can be considered more stable, because only those perturbations which are in phase over the duration of the relaxation time can change  $\chi_{\rm NL}$  appreciably. However, when the pulse becomes longer, the behavior of this solution should approach the time-independent solution. We integrated numerically Eqs. (1) and (2) for Gaussian input pulses

$$E = E_0 \exp[-(t^2/2T^2) - (r^2/2)], \tag{9}$$

for pulse lengths up to 20 times the relaxation time (T = 10). The result shows that for shorter pulses the trapping is stable and that the above description is qualitatively correct.

Figures 5 and 6 show typical results for a short pulse. The input peak power is  $5.4 P_{\rm th}$ , or  $|E|^2 = 0.045$  and the duration T = 1.5. Figures 5(a) and (b) show the intensity at the center and the width viewed at various distances in the medium as a function of local time. They are normalized to the input values. The distances are

chosen at equal intervals z = 0.0666n, where n runs from one to eight. The top curve corresponds to n = 1and the bottom to n = 8. The zero in the horizontal scale indicates the center of the input pulse and the left side corresponds to the front. Except for the accompanying oscillation, trapping of the pulse is clearly indicated. At the tail the radius shrinks to approximately 1/20th of the input value at around z = 0.2, and remains at practically the same value until z = 0.666, where the calculation was terminated. Accordingly, the intensity at the center increases approximately 100 times in this part of the pulse. Although intensity and radius are not completely constant, the latter part of the pulse with duration T =1.5 can be considered as a filament. The frequency spectra at the center and at z = 0.533 are shown in Fig. 6. This distance corresponds to the n = 8 curve in Fig. 5. It reproduces fairly well the spectrum observed in CS<sub>9</sub>. The spectrum is also quite similar to that obtained by one-dimensional calculation [14]. No appreciable radial variation is found in the filament spectrum [35]. This result is expected since the different parts of the beam cross-section are constantly being mixed by diffraction in a trapped beam.

The oscillations in intensities and radii in Fig. 5 appear in all numerical solutions shown in this paper and are well correlated to each  $2\pi$  phase shift in the field E. The oscillation starts because of a time lag between the wavefront distortion and the radial contraction. When the pulse is focusing, the wavefront is concave in the propagation direction and remains concave until the radius contracts beyond its stationary value. Then diffraction gradually bends the wavefront in the opposite direction. The radius, therefore, always undershoots at the focal point before expanding again. This behavior is also seen in the time-independent solutions discussed in the last section. However, with finite relaxation time the nonlinear index  $\chi_{NL}$  does not follow rapid changes in the field intensity. Contrary to the time-independent solution, the radius does not expand much beyond its stationary value; this expansion is usually 10 to 20 percent of the filament radius. As the pulse propagates farther, the radius continues to oscillate by approximately the same amount instead of approaching a stationary value. This is probably due to the difference in phase modulation among various radial parts of the pulse. In the steady state solution Eq.(7), the phase in the wing exactly follows the phase at the beam center. However, in the above numerical solution, the phase in the far wings is found to be constant, independently of  $t - z/v_a$ . Since phase modulation accumulates at beam center, the wavefront is inevitably distorted.

Calculation on a shorter pulse with T=0.5 shows similar results. With a peak power input of 12  $P_{th}$ , the radius contracts to approximately 1/15 and the pulse

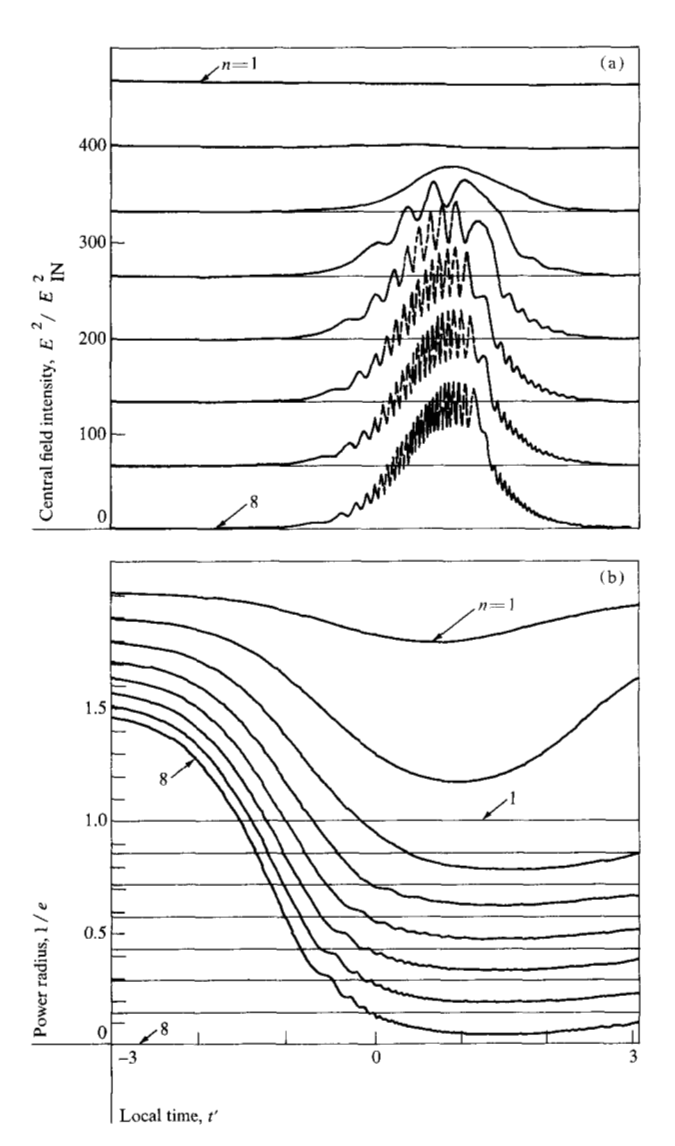
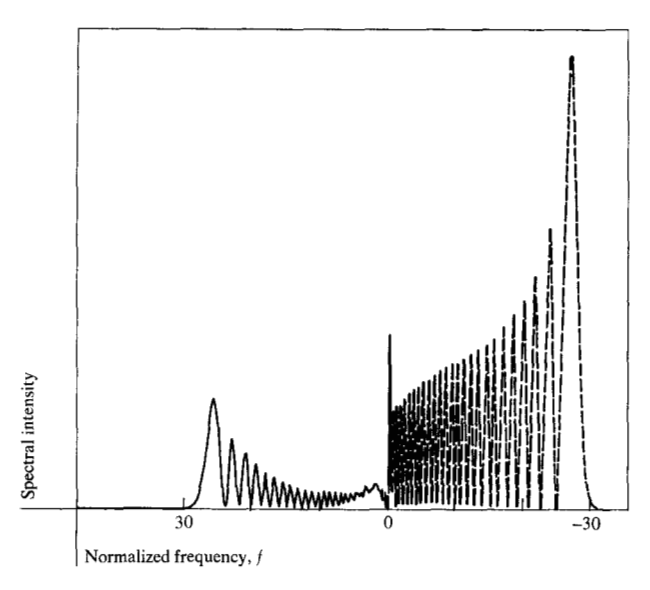


Figure 5 (a) The intensity at the center and (b) the 1/e radius of a pulse with duration T = 1.5 and power  $5.4 P_{th}$ . The lines are at distances z = 0.0666 n, where  $n = 1, 2, \dots, 8$ . Zero in the horizontal scale corresponds to the center of the input pulse. The base lines were shifted vertically as shown to improve visibility.

forms a filament of length 0.6. A pulse of duration T=5 with input power 2.4  $P_{\rm th}$  forms a filamentary structure of length three. For a longer pulse the tail part of the filament seems to be less stable. For a pulse of duration T=10 with power 1.7  $P_{\rm th}$ , the tail of the filament diverges after passing through the focal points. Even when it does diverge the preceding part of the filament remains trapped and propagates stably.

# • Effects of input power

The filament length changes only slowly with input power. However, the filament radius decreases very rapidly with increasing power, and the relation between the



**Figure 6** The frequency spectrum at a distance z = 0.533, corresponding to the n = 8 line in Fig. 5. Zero designates the original laser frequency. The frequency f is normalized to the relaxation time.

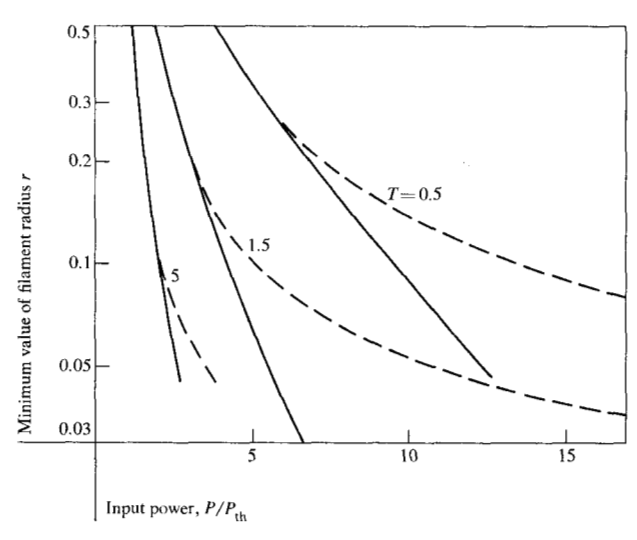


Figure 7 The change in absolute minimum radius with input power for various input pulse lengths. The radius is measured at the peak of the central field intensity  $|E|^2$ . The dashed line is the radius at which the peak of the pulse reaches its first minimum and decreases again. The minimum radius decreases more rapidly for a long pulse.

minimum radius and the power is shown for three pulse lengths in Fig. 7. The radius decreases almost exponentially with power, which is to be expected from the steady state solution in Eq. (7). Therefore, it is clear that the physical radius of the filament would soon become extremely small as the input power is raised. However, the observed filament radius is much smaller than that which is calculated from the known value for the reorientational Kerr effect. The most plausible explanation is that the pulse is cut off by nonlinear absorption or scattering when its radius becomes smaller than a critical

radius  $r_c$  of a few micrometers. The preceding part of the pulse has the observed radius and remains trapped.

The propagation of a pulse with arbitrary input power can be described as shown schematically in Fig. 8. The horizontal scale indicates the position in the pulse by the local time  $t' = t - z/v_q$ . The heavier solid line is the trajectory of the destructive point at which the radius becomes smaller than the critical radius  $r_e$ . The heavy line starts at the distance  $z = z_3$  and from the position  $t' = t_3'$ . The energy in the neighborhood of this point is dissipated either by nonlinear absorption or by scattering. As the pulse propagates, this destructive point advances towards the front or possibly towards the back. The heavy line corresponds to the trajectory of moving foci in the time-independent theory [2]. When the destructive point advances to  $t_2'$  at  $z = z_2$ , the minimum radius becomes larger than  $r_{\rm c}$  and the destructive point ceases to exist.

The propagation of the portion  $t' < t_2'$  is the same as that of the "well-behaved" pulse previously described. The portion between  $t_1'$  and  $t_2'$ , which has a length of the order of one and has approximately a constant radius of the order of  $r_c$ , can be considered as being a filament. This filament gradually expands and disappears at around the diffraction length  $z_d$  of the leading edge. The boundary of the filament cannot be uniquely defined. One may extend the trajectory of the moving foci beyond  $t_{a}$  by defining it as the trajectory of the point at which the radius attains its minimum value. At the front edge of the pulse this trajectory ends at the linear focal distance and for our input condition is z = 0. This portion, however, shown by a dashed line in Fig. 8, does not represent the front edge of the filament. Particularly in a short pulse, the trajectory disappears at a distance much shorter than  $z_d$ . For a long pulse the minimum radius decreases very rapidly with power above  $P_{th}$ . Therefore most of the pulse contracts to a radius smaller than  $r_{\rm c}$ . In addition,  $z_2$  is very large, because the self-focusing distance diverges at  $P = P_{th}$  for an infinitely long pulse. Therefore the destructive point is observed at any distance in the medium. As the input pulse becomes shorter, the distance  $z_2 - z_3$  shortens and  $z_2$  decreases. As a result the probability of observing filaments increases.

Figures 9 and 10 show the result with  $|E|^{16}$  loss, which represents a sharp cutoff. The duration of the input pulse is T=3 and the power is  $12.1\,P_{\rm th}$ . A loss term  $-2\times 10^{-6}i|E|^{16}$  is added to the right side of Eq. (1). Figure 9 shows the central intensity at various distances. The curve for z=0.088 corresponds approximately to the distance at which the first focal point is formed. Since the pulse length is relatively short, the focal point quickly spreads to both sides of the pulse. The tail part is cut off due to the disturbance caused by the nonlinear loss. The part of the pulse for which -2 < t' < 1, re-

mains trapped and propagates. Figure 10 shows the spectrum at the same distances as in Fig. 9. The spectrum has large components around the original frequency and is complicated compared to the well-behaved filament shown in Fig. 6.

In these examples the filament sizes were selected to be approximately 0.05. For a T=1.5 pulse, a larger power of 8  $P_{\rm th}$  was also tried. The stability of the trapping was not affected by this larger power. However, the evolution towards the final radius is more complicated in this case. The spectral broadening starts well before the radius reaches its final size [37]. The radius of the portion that shrinks fastest hits the first minimum when the frequency begins to broaden. Then the pulse gradually approaches its absolute minimum radius by reaching repeated minima and maxima. The relation between the radius at the first minimum and the input power is shown in Fig. 7 by dashed lines. This radius tends to saturate with power.

In principle, the contraction ratio of the radius can be estimated from Fig. 7 if the filament power and the duration are known. Actually this is rather difficult to estimate in view of the rapid change of radius with power. Typical filaments in CS<sub>2</sub> produced by mode-locked Nd lasers have 1 ps duration [15] and 400 GW/cm<sup>2</sup> power density [38]. This means that the filament radius is approximately 0.1. If the input power is twice as large, it is reduced to 0.01. These values are often still larger than the ratios of the radii of the filaments to that of the laser beams in usual experimental conditions. However it is known that, in multimode lasers, the self-focusing starts from hot spots much smaller than the beam diameter [39,40].

We have shown in the last section that only a fraction of the beam power self-focuses in the time-independent solutions. A similar behavior is found for the transient focusing, which is very critical to the time dependence of the input pulse. When the pulse is square, the situation is similar to that for time-independent focusing. If the pulse, is triangular, however, with a ramp speed dP/dt equal to several times the numerical value of  $P_{\rm th}$ , most of the power is trapped. For the pulse in Fig. 5, more than half of the beam power is trapped in the filament.

## Stimulated Raman scattering and dispersion

The results in the preceding sections do not include two important effects that usually accompany the filaments produced by short pulses. These effects are stimulated Raman scattering and linear dispersion. In most cases a strong Raman-Stokes component is observed in filaments. The importance of stimulated Raman scattering does not decrease for short pulses, since the Raman process is usually faster than the reorientational Kerr

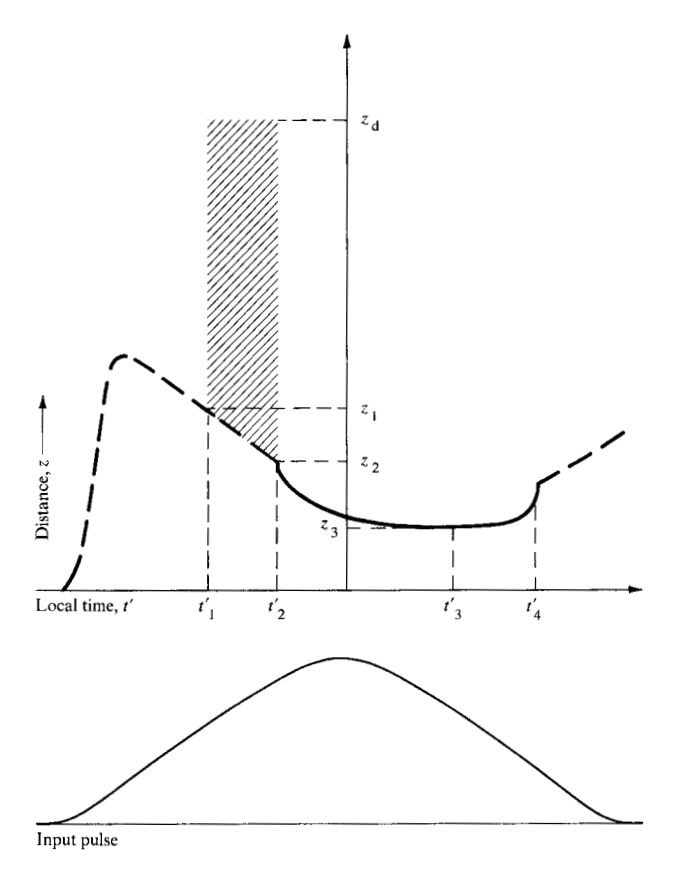


**Figure 8** A schematic diagram explaining the moving foci (thick line) and the filament (shaded area) for a short pulse. The solid line is the destructive track. The dashed line is the locus of the well-behaved minimum radius. Local time  $t' = t - \frac{z}{v_g}$ .

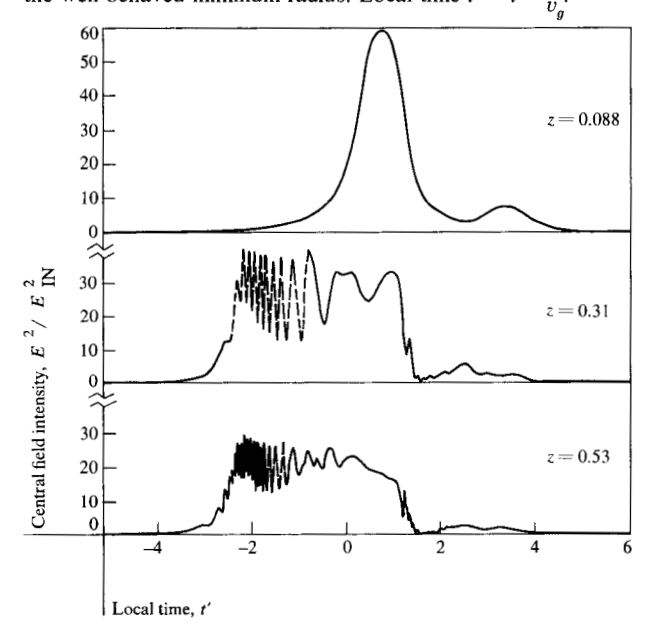


Figure 9 The propagation of a pulse with tail cut off by a sharp nonlinear loss. The pulse length is T = 3 and the power is 12  $P_{\text{th}}$ . The loss is proportional to  $|E|^{16}$ . The top curve corresponds approximately to the distance at which the first focal point is formed. Local time t' is normalized to the relaxation time of the Kerr nonlinearity.

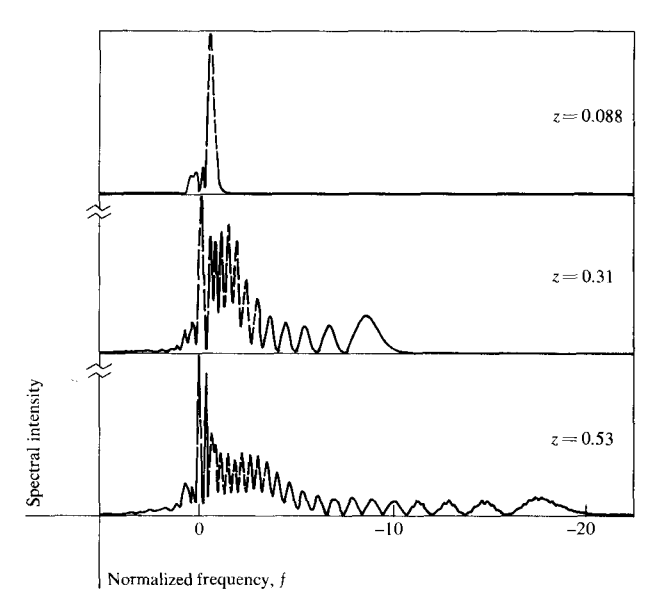


Figure 10 The development of the frequency spectrum for the data in Figure 9. Zero designates the original laser frequency.

effect in liquids. In the absence of frequency broadening, and for a pulse longer than several picoseconds, dispersion would not have a large effect on pulse propagation over several centimeters. However, the intense, trapped part of the pulse produces a large frequency broadening. The new frequency components start to distort the filament envelope by dispersion. In considering the effect on filament stability by these disturbances, one should note that the filament is supported by the refractive index change created by the preceding "horn" (see Fig. 3), which has less intensity. These disturbances, on the other hand, are initially created inside the filament. Therefore, if the disturbances do not affect the horn, the filament may be treated approximately as a light pulse that is trapped and propagates in a dielectric waveguide. Planewave theories will describe qualitatively the filament propagation. Such theories have been discussed in detail for the pulse distortion due to nonlinear refractive index [31,41,42] as well as for the transient stimulated Raman effect [43-48]. If the disturbances affect the horn, the results will be qualitatively different from those of one-dimensional theories.

The main purpose of this section is to consider the stability of the filament itself. Because of the large number of parameters involved in these processes, it is rather difficult to investigate numerical solutions for a wide range of conditions, and so only two examples are included.

First we consider the effect of Raman-Stokes wave generation with a large frequency shift, as in the C-H stretching mode. We add to Eq. (1) an equation for the propagation of the Raman-Stokes field  $E_8$ :

$$\left[\frac{\partial}{\partial z} + \left(\frac{1}{v_g} - \Delta\right) \frac{\partial}{\partial t}\right] E_{\rm S} = \frac{\omega_0}{\omega_0 - \omega_{\rm v}} \left(\frac{\partial^2}{\partial r^2} + \frac{1}{r} \frac{\partial}{\partial r}\right) E_{\rm S} + i \frac{\omega_0 - \omega_{\rm v}}{\omega_0} \chi_{\rm NL} E_{\rm S}, \tag{10}$$

in which  $\Delta$  is the group velocity mismatch.

The nonlinear susceptibility  $\chi_{\rm NL}$  is now the sum of two contributions

$$\chi_{\rm NL} = \chi_{\rm ID} + \chi_{\rm R},\tag{11}$$

where  $\chi_{ID}$  is the nonlinear refractive index and  $\chi_R$  is the Raman susceptibility. These are governed by the equations

$$(\partial \chi_{\text{ID}}/\partial t) + \chi_{\text{ID}} = |E|^2 + |E_{\text{S}}|^2, \tag{12}$$

$$(\partial \chi_{\rm R}/\partial t) + \left(\frac{1}{\tau_{\rm R}} + i\omega_{\rm v}\right)\chi_{\rm R} = g_{\rm R}E E_{\rm S}^*. \tag{13}$$

This formulation assumes that the degree of frequency broadening is much smaller than the vibrational frequency  $\omega_v$ . Linear dispersion is taken into account in the lowest-order approximation through the group velocity mismatch  $\Delta$ . In most liquids these assumptions provide sufficiently good approximations if the input pulse is longer than a few picoseconds. The additional equations (10) through (13) will affect the solution in the following way. The nonlinear refractive index  $\chi_{\rm ID}$  decreases by a factor  $(\omega_0 - \omega_v)/\omega_0$  as the laser field E is converted into the Stokes field  $E_{\rm S}$ . This change in  $\chi_{\rm ID}$  will advance towards the leading edge of the pulse as  $E_{\rm S}$  advances because of the group velocity mismatch  $\Delta$ .

Equations (1) and (10) through (13) were integrated with input conditions T=1.5 and  $P=5.4\,P_{\rm th}$ , which are the same as those of Fig. 5. A constant value of  $5.4\times 10^{-20}P_{\rm th}$  was taken for the input of  $|E_{\rm S}|^2$ . Other parameters were chosen as follows:.  $\Delta=0.01666$ ,  $g_{\rm R}=8$ ,  $\tau_{\rm R}=0.2$ , and  $(\omega_0-\omega_{\rm v})/\omega_0=0.792$ . The latter value corresponds to a vibrational mode of 3000 cm<sup>-1</sup> for a ruby laser. The other parameters are chosen so that  $E_{\rm s}$  grows sufficiently fast compared to the frequency broadening and that it advances into the horn before the filament disappears by diffraction. Figure 11 shows the development of the laser pulse and Fig. 12 that of the Stokes pulse.

The Stokes pulse starts to grow from the tail of the filament as the filament is formed (n=1). It gradually depletes the laser field from the tail of the filament (n=2). At this stage the nonlinear refractive index  $\chi_{\rm ID}$  is already substantially affected by conversion of the laser field into a Stokes field. However, the filament radius retains its size approximately, because the horn is not yet affected. The Stokes field advances relative to the laser field because of group velocity dispersion. The Stokes field gradually thrusts into the horn and depletes

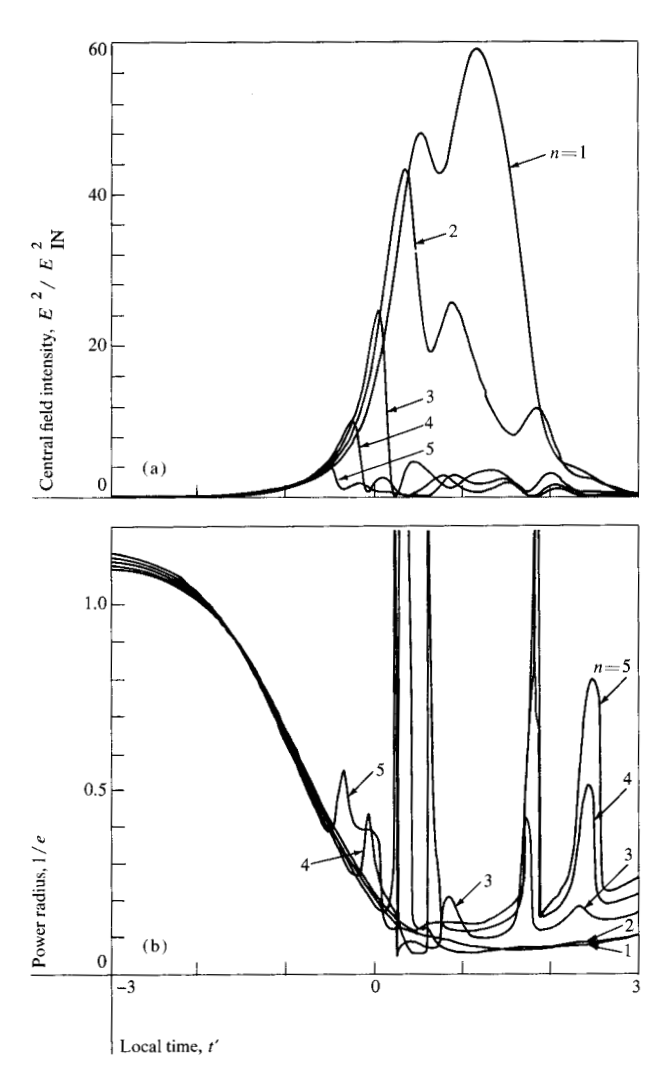


Figure 11 Propagation of a filament in the presence of strong stimulated Raman scattering. (a) The intensity at the center of the laser field; (b) the 1/e power radius. Five curves are at distances z = 0.2 + 0.011 n, where  $n = 1, 2, \dots, 5$ . The input pulse is of length T = 1.5 and power P = 5.4  $P_{th}$ .

the laser field (n=3,4 and 5). Then the filament radius starts to expand rapidly, which may be seen especially clearly in the Stokes component in Fig. 12. The small leftover energy of the laser component becomes extremely unstable, because the refractive index change created by the expanded Stokes filament cannot maintain the laser component at its original size. If the velocity mismatch  $\Delta$  is set to zero, the Stokes component does not advance beyond the front of the filament, where stability is not affected. This stability was confirmed by an independent integration using the same values for the other constants.

In some liquids the frequency broadening often exceeds the Raman shift. In this case the Raman and laser fields cannot be artificially separated. Numerical integration becomes extremely time-consuming because a very

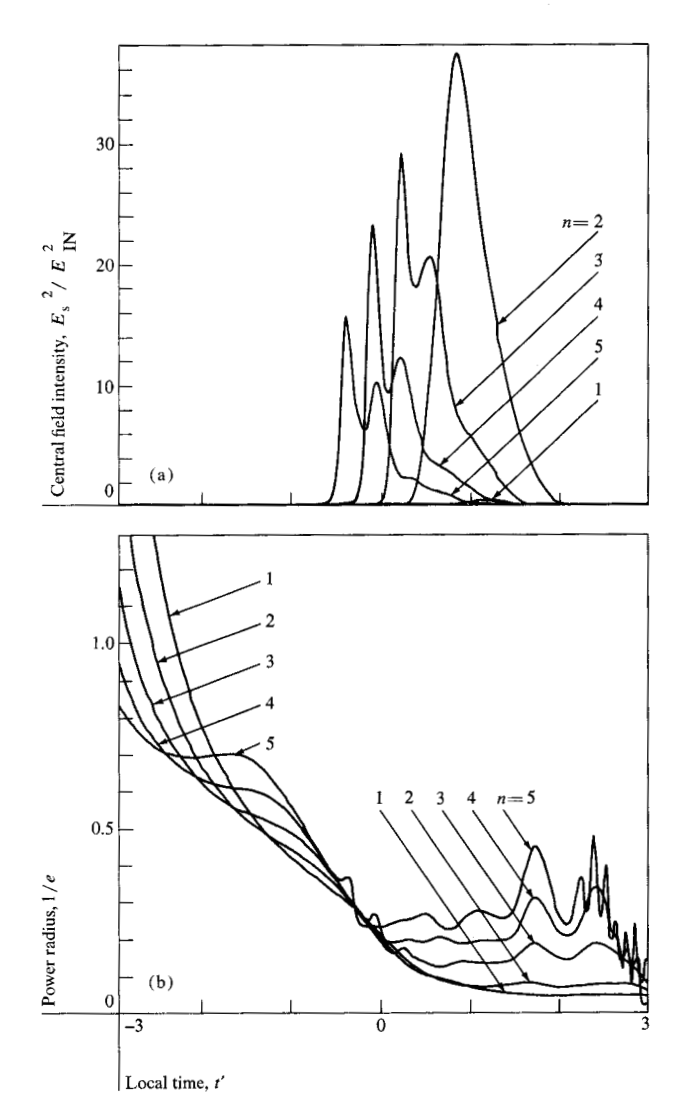


Figure 12 The development of the Stokes field in the pulse represented in Fig. 11. As the Stokes filament advances into the horn, the radius expands to the horn size at the front edge of the Stokes filament.

fine grid size is required on the time axis. We consider the following equations, which include dispersion and stimulated Raman scattering in the simplest form:

$$\left(\frac{\partial}{\partial z} + \frac{1}{v_g} \frac{\partial}{\partial t}\right) E = \left(\frac{\partial^2}{\partial r^2} + \frac{1}{r} \frac{\partial}{\partial r}\right) E + i \left(1 + \frac{1}{\omega_0} \frac{\partial}{\partial t}\right) \chi_{NL} E 
- i \Delta' \frac{\partial^2 E}{\partial t^2},$$
(14)

$$\chi_{\rm NL} = \chi_{\rm 1D} + \chi_{\rm R},\tag{15}$$

$$\frac{\partial \chi_{\rm ID}}{\partial t} + \chi_{\rm ID} = |E|^2,\tag{16}$$

$$\frac{\partial^2 \chi_{\rm R}}{\partial t^2} + \frac{2}{\tau} \frac{\partial \chi_{\rm R}}{\partial t} + \omega_{\rm v}^2 \chi_{\rm R} = g'_{\rm R} |E|^2. \tag{17}$$

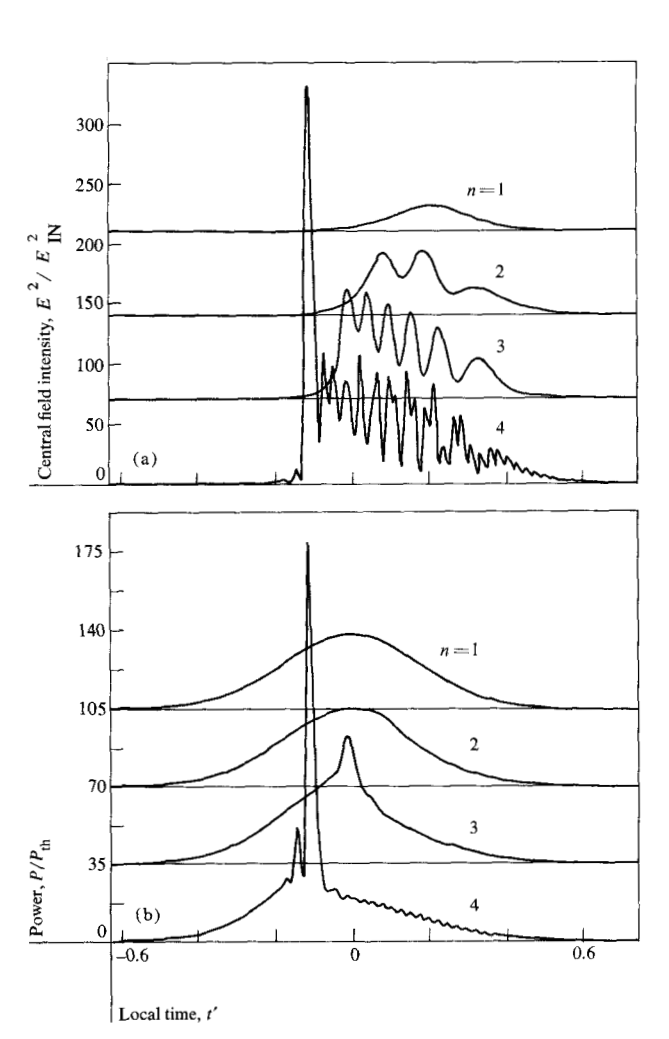


Figure 13 Effect of dispersion and stimulated Raman scattering on a very short filament. (a) Intensity at the center; (b) the power  $2\pi \int r |E|^2 dr$ . The curves are for distances z = 0.103 + 0.033 n, where n = 1, 2, 3 and 4. At n = 1 the filament has just formed. The input pulse has T = 0.25 and P = 35  $P_{\rm th}$ .

Here the slowly varying part of the field E is used to represent the entire field. For a better approximation, the first term on the right side of Eq. (14) would have to be multiplied by  $(1-\omega_0^{-1}\partial/\partial t)$ . This factor was neglected in our computations. For the parameters selected in the following numerical example, this factor, as well as  $(1+\omega_0^{-1}\partial/\partial t)$  in the second term, does not have a large effect on pulse propagation. However, the latter was retained in order to insure the proper reduction in  $|E|^2$  as the frequency is shifted downwards. The last term in Eq. (14) represents linear dispersion. The Raman susceptibility  $\chi_R$  is governed by Eq. (17).

We integrated these equations for relatively small  $\omega_{\rm v}$ , so that the integration was feasible. The input pulse had a Gaussian shape with T=0.25 and a power of  $35P_{\rm th}$ . The values of the constants were chosen so that the solution simulated approximately the filament propagation

of a Nd mode-locked laser pulse. These were  $\omega_0 = 3900$ ,  $\omega_v = 271$ ,  $\Delta' = -2.5 \times 10^{-5}$ ,  $\tau = 10$ , and  $g_R' = 400$ . Figure 13 (a) shows the center intensity and 13 (b) the power  $2\pi \int r|E|^2 dr$ . Figure 14 shows the radius and Fig. 15 the frequency spectrum. To reduce calculation time, the dispersion term in Eq. (14), and the stimulated Raman effect in Eq. (17), were introduced after the first focal point was formed at  $z \approx 0.1$ .

The change in the central intensity qualitatively agrees with a one-dimensional calculation [49]. At extremely high intensities pulses deform in such a way as to form a shock at the tail because of the intensity-dependent refractive index [41]. In the intensity range of the filaments, the linear dispersion is found to be more important to pulse distortion [42,49] than is refractive index. For a short filament most of the pulse experiences a downward frequency shift and this portion advances. The pulse first becomes triangular and then produces a sharp spike at its leading edge. This spike soon disappears, but the shock continues to advance. The pulse distortion does not necessarily cause a decrease in the nonlinear refractive index  $\chi_{ID}$ , since the frequency shift is small compared to  $\omega_0$ . Therefore the filament radius does not expand immediately, even after the horn has begun to distort. The filament radius begins to be seriously disturbed at the distance at which the shock reaches the front of the pulse. Because the frequency broadening is large compared to the grid size for our integration, the last curve may not be accurate. Nevertheless, it is believed to show the general tendency of the pulse shape.

## Conclusion

The moving-foci model of self-focusing assumes implicitly that the focused beam diverges beyond its focal point, a characteristic substantiated by solutions of the time-independent equations. The model is successful in explaining the streaks of scattered light observed with single-mode lasers [1]. The assumption of beam divergence beyond its focal point, however, is not correct in all cases. We have shown that the inclusion of a finite relaxation time allows the beam to be trapped in the best conceivable sense for a beam of finite duration. The properties of the resulting filaments do not contradict the existing experimental observations.

The present results, however, do not explain the observed filament size of several micrometers. Various saturation mechanisms have been proposed for this observation [26, 50-52]. An important conclusion of our numerical integrations is that not only can a simple saturation of the nonlinear refractive index serve as a mechanism to limit the filament radius, but also that any nonlinear scattering or absorption can provide the mechanism.

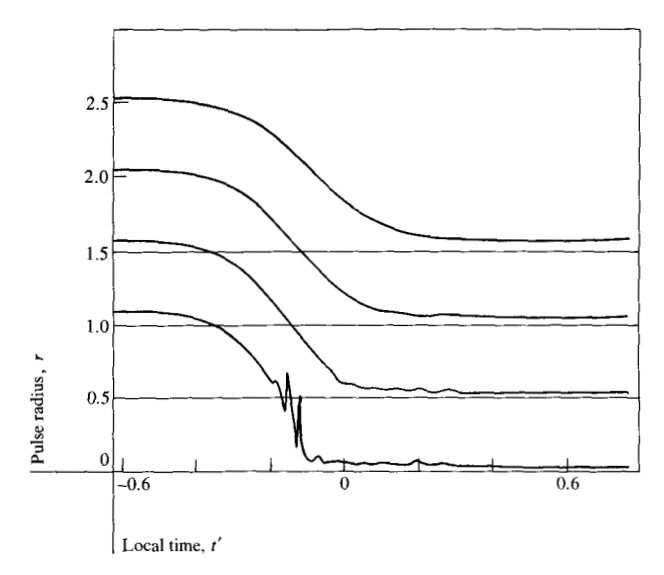


Figure 14 The development of the radius for the pulse shown in Fig. 13.



The author thanks E. Courtens for many helpful discussions. He is also grateful to N. Bloembergen, R. L. Carman and J. A. Fleck for useful discussions and exchange of information on their results prior to publication. The author is also indebted to M. McDonald for technical assistance with the computer programming.

#### References and notes

- V. V. Korobkin, A. M. Prokhorov, R. V. Serov, and M.Ya. Shchelev, ZhETF Pis. Red. 11, 153 (1970), [English translation, Sov. Phys. – JETP Lett. 11, 94 (1970)].
- M. M. T. Loy and Y. R. Shen, Phys. Rev. Letters 25, 1333 (1970).
- 3. Y. R. Shen and M. M. T. Loy, Phys. Rev. A 3, 2099 (1971).
- 4. J. A. Fleck, Jr. and P. L. Kelley, Appl. Phys. Letters 15, 313 (1969).
- K. A. Brueckner and S. Jorna, *Phys. Rev. Letters* 17, 78 (1966).
- V. I. Bespalov and V. I. Talanov, ZhETF Pis. Red. 3, 471 (1966), [English translation, Sov. Phys.-JETP Letters 3, 307 (1966)].
- 7. K. A. Brueckner and S. Jorna, Phys. Rev. 164, 182 (1967).
- 8. K. Grob and M. Wagner, Phys. Rev. Letters 17, 819 (1966).
- 9. Y. R. Shen, M. Y. Au Yang, and M. L. Cohen, *Phys. Rev. Letters* 19, 1171 (1967).
- V. E. Zakharov, Zh. Eksp. Teor. Fiz. 53, 1735 (1967)
   [English translation, Sov. Phys. JETP 26, 994 (1968)].
- P. Lallemand and N. Bloembergen, Phys. Rev. Letters 15, 1010 (1965).
- R. Y. Chiao, M. A. Johnson, S. Krinsky, H. A. Smith, C. H. Townes, and E. Garmire, *IEEE J. Quantum Electronics* QE-2, 467 (1966).
- 13. F. Shimizu, Phys. Rev. Letters 19, 1097 (1967).
- T. K. Gustafson, J. P. Taran, H. A. Haus, J. R. Lifsitz, and P. L. Kelley, *Phys. Rev.* 177, 306 (1969).
- 15. J. Reintjes, R. L. Carman, and F. Shimizu, to be published.
- M. M. Denariez-Roberge and J-P. E. Taran, Appl. Phys. Letters 14, 205 (1969).

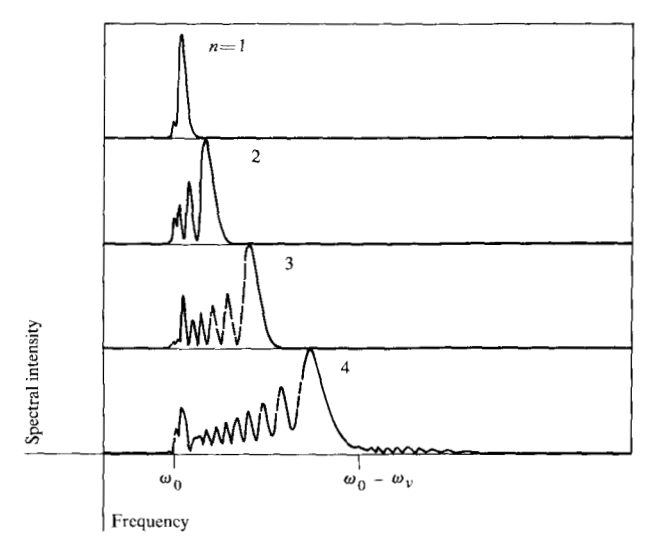


Figure 15 The development of the frequency spectrum for the pulse shown in Fig. 13. The far curves are at distances z = 0.103 + 0.033n, where n ranges from 1 to 4.  $\omega_0$  is the laser frequency and  $\omega_0 - \omega_n$  is the first Raman-Stokes frequency.

- R. Cubeddu, R. Polloni, C. A. Sacchi, O. Svelto, and F. Zaraga, Phys. Rev. Letters 26, 1009 (1971).
- 18. M. M. Paillette, Compt. Rend. 267, 29 (1968).
- 19. E. Garmire, Phys. Letters 17, 251 (1965).
- C. A. Sacchi, C. H. Townes, and J. R. Lifsitz, *Phys. Rev.* 174, 439 (1968).
- R. Y. Chiao, E. Garmire, and C. H. Townes, *Phys. Rev. Letters* 13, 479 (1964).
- 22. P. L. Kelley, Phys. Rev. Letters 15, 1005 (1965).
- E. Courtens, IEEE J. Quantum Electronics QE-7, 578 (1971).
- 24. C. C. Wang, Phys. Rev. Letters 16, 344 (1966).
- 25. A. Piekara, IEEE J. Quantum Electronics QE-2, 249 (1966).
- 26. T. K. Gustafson, P. L. Kelley, R. Y. Chiao, and R. G. Brewer, *Appl. Phys. Letters* 12, 165 (1968).
- S. A. Akhmanov, A. P. Sukhorukov, and R. V. Khokhlov, Zh. Eksp. Teor. Fiz. 50, 1537 (1966). [English translation, Sov. Phys. – JETP 23, 1025 (1966)].
- E. L. Dawes and J. H. Marburger, Phys. Rev. 179, 862 (1969).
- The results in Figs. 1 and 2 reconfirm qualitatively the conclusion by Dyshko et al. that the beam focuses in units of Pth at different distances. A. L. Dyshko, V. N. Lugovoi and A. M. Prokhorov, ZhETF Pis. Red. 6, 655 (1967), [English translation, Sov. Phys.—JETP Letters 6, 146 (1967)].
- S. A. Akhmanov, A. P. Sukhorukov, and R. V. Khokhlov, *Usp. Fiz. Nauk* 93, 19 (1967) [English translation, Sov. *Phys. Usp.* 10, 609 (1968)].
- S. A. Akhmanov, A. P. Sukhorukov, and R. V. Khokhlov, *Zh. Eksp. Teor. Fiz.* 51, 296 (1966) [English translation, *Sov. Phys. – JETP* 24, 198 (1967)].
- V. A. Aleshkevich, S. A. Akhmanov, A. P. Sukhorukov, and A. M. Khachatryan, ZhETF Pis. Red. 13, 55 (1971) [English translation, Sov. Phys.-JETP Letters 13, 36 (1971)].
- N. Bloembergen, Fundamental and Applied Laser Physics, Proceedings of the Esfahan (Iran) Symposium. Editors:
   M. S. Feld, N. A. Kurnit, and A. Javan, John Wiley and Sons, New York. (To be published).
- 34. R. V. Khokhlov, Proceedings cited in Ref. 33.

- 35. F. Shimizu and E. Courtens, Proceedings cited in Ref. 33.
- J. A. Fleck and R. L. Carman, Appl. Phys. Letters 20, 290 (1972).
- 37. The same behavior is observed in the calculation by Fleck et al., Ref. 36.
- 38. R. G. Brewer and C. H. Lee, *Phys. Rev. Letters* 21, 267 (1968).
- Yu. S. Chilingarian, Zh. Eksp. Teor. Fiz. 55, 1589 (1968)
   [English translation, Sov. Phys. JETP 28, 832 (1969)].
- 40. S. C. Abbi and H. Mahr, *Phys. Rev. Letters* **26**, 604 (1971).
- F. DeMartini, C. H. Townes, T. K. Gustafson, and P. L. Kelley, *Phys. Rev.* 164, 312 (1967).
- R. A. Fisher and P. L. Kelley, Appl. Phys. Letters 14, 140 (1969).
- 43. N. M. Kroll, J. Appl. Phys. 36, 34 (1965).
- S. A. Akhmanov, A. S. Chirkin, K. N. Drabovich, A. I. Kovrigin, R. V. Khokhlov, and A. P. Sukhorukov, *IEEE J. Quantum Electronics* QE-4, 598 (1968).
- 45. C. S. Wang, Phys. Rev. 182, 482 (1969).
- R. L. Carman, F. Shimizu, C. S. Wang, and N. Bloembergen, *Phys. Rev. A* 2, 60 (1970).
- A. P. Sukhorukov and A. K. Shchednova, Zh. Eksp. Teor. Fiz. 60, 1251 (1971), [English translation, Sov. Phys. – JETP 33, 677 (1971)].

- 48. N. M. Kroll and P. L. Kelley, Phys. Rev. A, 4, 763 (1971).
- 49. F. Shimizu, IEEE J. Quantum Electronics QE-8, 851 (1972).
- 50. E. Yablonovitch and N. Bloembergen, *Phys. Rev. Letters* 29, 907 (1972).
- 51. T. K. Gustafson and C. H. Townes, *Phys. Rev. A*, **6**, 1659 (1972).
- 52. O. Rahn and M. Maier, Phys. Rev. Letters 29, 558 (1972).

Received October 6, 1972

The author is located at the Department of Applied Physics, The University of Tokyo, Bunkyo-ku, Tokyo, Japan. The work reported in this paper was done at the IBM Zurich Research Laboratory, 8803 Rüschlikon, Switzerland.